Iron(III) Spin-Crossover Compounds with a Wide Apparent Thermal Hysteresis around Room Temperature

Shinya Hayami,[†] Zhong-ze Gu,[†] Hajime Yoshiki,[‡] Akira Fujishima,[§] and Osamu Sato*,[†]

Contribution from the Special Research Laboratory for Optical Science, Kanagawa Academy of Science and Technology, East 412, 3-2-1 Sakado, Takatsu-ku, Kawasaki-shi, Kanagawa 213-0012, Japan, RIKEN Hirosawa, Wako, Saitama 351-0198, Japan, and Department of Applied Chemistry, The University of Tokyo, 7-3-1 Hongo, Bunkyo-ku, Tokyo 113-8656, Japan

Received May 23, 2000. Revised Manuscript Received August 28, 2001

Abstract: The magnetic properties of the spin-crossover compounds, $[Fe(qsal)_2]NCSe\cdot MeOH$ (**1**) and $[Fe(qsal)_2]NCSe\cdot CH_2Cl_2$ (**2**), have been measured. We have discovered that both compounds **1** and **2** exhibit a wide thermal hysteresis loop of 140 K ($T_{1/2}\uparrow = 352$ K and $T_{1/2}\downarrow = 212$ K) and 180 K ($T_{1/2}\uparrow = 392$ K and $T_{1/2}\downarrow = 212$ K), respectively, in the first cycle. Thermogravimetric analysis shows that solvent molecules escape from compounds **1** and **2** around 340 and 395 K, respectively. This means that the hysteresis loops observed for the first cycle are only apparent ones. Following the first loop, they show a two-step spin-crossover in warming mode. The so-called "step 1" and "step 2" are centered around $T_{1/2(S1)}\uparrow = 215$ K and $T_{1/2(S2)}\uparrow = 282$ K, respectively. On the other hand, a one-step spin-crossover occurs at $T_{1/2}\downarrow = 212$ K in cooling mode. The hysteresis widths can be estimated to be 3 K (step 1) and 70 K (step 2), assuming that the widths in steps 1 and 2 are defined as the differences between $T_{1/2(S1)}\uparrow$ and $T_{1/2}\downarrow$, and $T_{1/2(S2)}\uparrow$ and $T_{1/2}\downarrow$, respectively. The hysteresis width of 70 K in step 2 is one of the widest values reported so far for spin-crossover complexes. It is thought that the cooperativity operating in the complexes arises mainly from the intermolecular π interactions between quinoline and phenyl rings. Using a previously repored model, we are able to simulate the hysteresis loop with a two-step spin-crossover in warming mode and a one-step transition in cooling mode.

Introduction

The design of molecules that could be utilized for information processing and information storage is one of the main challenges in molecular materials science. The molecules that would be suitable for such applications must exhibit bistability, which may be defined as a property of a molecular system that allows it to exist in two different electronic states over a certain range of external perturbation. A typical example of a molecular species that exhibits such a molecular bistability is spin-crossover compounds. Since the discovery of the first spin-crossover compound,[1,2] a variety of d^n ($n = 4-7$) transition metal compounds exhibiting bistability between the high-spin (HS) and low-spin (LS) states have been reported.[3−5] Usually, the spin transition phenomena can be induced by a variation of temperature or of pressure. On the other hand, Decurtins et al. showed in 1984 that the spin transition could be induced by illumination.[6] This finding shows that spin-crossover compounds have potential applications as optical switches and data storage devices.[6,7]

The spin-crossover phenomenon depends strongly on intermolecular interactions.[8] When the magnitude of these intermolecular interactions overcomes a threshold value, the spin-crossover phenomenon becomes cooperative. In such a case, the spin transitions between the LS and HS states may not only be very abrupt but may also occur with a hysteresis effect. The presence of the hysteresis effect is important, because a molecular compound that exhibits hysteresis can take two different electronic states between $T_{1/2}\uparrow$ and $T_{1/2}\downarrow$ depending on its history, enabling the fabrication of information storage and processing devices. Note that $T_{1/2}\uparrow$ and $T_{1/2}\downarrow$ are defined as the temperatures for which there are 50% high-spin and 50% low-spin states in the warming and cooling modes, respectively. A compound with a large thermal hysteresis at room temperature needs to be developed for practical applications.[9] Although many attempts have been made to produce a suitable compound in previous studies, so far the production of spin-crossover compounds with such a wide hysteresis is still a challenging issue. Here, we show that the mononuclear iron(III) compounds, $[Fe(qsal)_2]NCSe\cdot MeOH$ (**1**) and $[Fe(qsal)_2]NCSe\cdot CH_2Cl_2$ (**2**), where Hqsal is the abbreviation for *N*-(8-quinolyl)salicylaldimine, exhibit a $S = {}^5/_2$ (HS) $\rightleftarrows S = {}^1/_2$ (LS) spin transition with a wide thermal hysteresis. Furthermore, we report on a novel thermal hysteresis loop, i.e., a one-step transition in cooling mode and a two-step transition in warming mode.

[†] Kanagawa Academy of Science and Technology.
[‡] RIKEN Hirosawa.
[§] The University of Tokyo.

(1) Cambi, L.; Cagnasso, A. *Atti Accad. Naz. Lincei* **1931**, *13*, 809.
(2) Cambi, L.; Szegö, L.; Cagnasso, A. *Atti Accad. Naz. Lincei* **1932**, *15*, 266.
(3) (a) Goodwin, H. A. *Coord. Chem. Rev.* **1976**, *18*, 293−325. (b) Gütlich, P. *Struct. Bonding (Berlin)* **1981**, *44*, 83−195. (c) Gütlich, P.; Hauser, A. *Coord. Chem. Rev.* **1990**, *97*, 1−22. (d) König, E. *Prog. Inorg. Chem.* **1987**, *35*, 527−623. (e) König, E. *Struct. Bonding (Berlin)* **1991**, *76*, 51.
(4) Maeda, Y.; Takashima, Y. *Comments Inorg. Chem.* **1988**, *7*, 41−52.
(5) Zarembowitch, J. *New J. Chem.* **1992**, *16*, 255−267.
(6) Decurtins, S.; Gütlich, P.; Köhler, C. P.; Spiering, H.; Hauser, A. *Chem. Phys. Lett.* **1984**, *105*, 1−4.
(7) Gütlich, P.; Hauser, A.; Spiering, H. *Angew. Chem., Int. Ed. Engl.* **1994**, *33*, 2024−2054.
(8) Hayami, S.; Gu, Z. Z.; Shiro, M.; Einaga, Y.; Fujishima, A.; Sato, O. *J. Am. Chem. Soc.* **2000**, *122*, 7126−7127.
(9) Kahn, O.; Kröber, J.; Jay, C. *Adv. Mater.* **1992**, *4*, 718−728.

10.1021/ja0017920 CCC: $20.00
Published on Web 11/03/2001

Experimental Section

Synthesis. The ligand *N*-(8-quinolyl)salicylaldimine (Hqsal) and $[Fe(qsal)_2]Cl$ were prepared from 8-aminoquinoline and salicylaldehyde according to the method described previously.[10,11] The compound $[Fe(qsal)_2]NCSe\cdot MeOH$ (**1**) was prepared by slow addition of a MeOH solution (30 mL) containing $[Fe(qsal)_2]Cl$ (0.5 mmol) to a MeOH solution (30 mL) containing an excess of KNCSe (2 mmol). Thin single crystals of **1** appeared in 2 days. Anal. Calcd for $C_{34}H_{26}O_3N_5Se_1Fe_1$ (**1**): C, 59.41; H, 3.81; N, 10.19; Fe, 8.12. Found: C, 59.21; H, 3.70; N, 10.20; Fe, 8.33. The compound $[Fe(qsal)_2]NCSe\cdot CH_2Cl_2$ (**2**) was prepared by the slow addition of $MeOH/CH_2Cl_2$ = 1:1 solutions (30 mL) containing $[Fe(qsal)_2]Cl$ (0.5 mmol) to $MeOH/CH_2Cl_2$ = 1:1 solutions (30 mL) containing an excess of KNCSe (2 mmol). Brown single crystals appeared in 2 days. The single crystals were washed with MeOH and dried in air. Anal. Calcd for $C_{34}H_{24}O_2N_5Cl_2Se_1Fe_1$ (**2**): C, 55.16; H, 3.27; N, 9.46; Fe, 7.54. Found: C, 55.35; H, 3.48; N, 9.49; Fe, 7.31. The solvent molecules in the crystals, MeOH and CH_2Cl_2, can be removed by annealing compounds **1** and **2** in vacuo at 400 K. The elemental analyses after removing the solvent molecules are as follows. Calcd for $C_{33}H_{22}O_2N_5Se_1Fe_1$: C, 60.48; H, 3.38; N, 10.69; Fe, 8.52. Found (for **1**): C, 60.25; H, 3.50; N, 10.57; Fe, 8.41. Found (for **2**): C, 60.32; H, 3.43; N, 10.60; Fe, 8.38.

Susceptibility Measurements. The magnetic susceptibilities $\chi(T)$ for compounds **1** and **2** between 5 and 400 K were measured with a superconducting quantum interference device (SQUID) magnetometer (Quantum Design MPMS-5S) in an external field of 0.5 T.

Mössbauer Spectroscopy. The Mössbauer spectra (isomer shift vs metallic iron at room temperature) were measured using a Wissel MVT-1000 Mössbauer spectrometer with a $^{57}Co/Rh$ source in the transmission mode. All isomer shifts are given relative to α-Fe at room temperature. The measurements at low temperature were performed with a closed-cycle helium refrigerator cryostat (Iwatani Co., Ltd.).

Crystallographic Data Collection and Structural Determination. The brown platelet-shaped crystals of **1** and **2** with approximate dimensions of 0.3 × 0.3 × 0.01 mm and 0.3 × 0.3 × 0.03 mm, respectively, were mounted in a glass capillary. The temperature of the crystals was slowly decreased from room temperature to 200 and 230 K for **1** and **2**, respectively, and then the X-ray structural analyses were carried out. All measurements were made on a Rigaku RAXIS−RAPID imaging plate diffractometer with graphite-monochromated Mo Kα radiation. Data were collected at 200 and 230 K to a maximum 2θ value of 55.0°. For compound **1**, of the 10 751 reflections that were collected, 6079 were unique (R_{int} = 0.066) and 2550 with $I > 3\sigma(I)$ were used to solve the structure with SIR92. The final R values gave $R1$ = 0.059 for $I > 3\sigma(I)$, R = 0.094 and R_w = 0.136 for all data, with a linear absorption coefficient μ(Mo Kα) = 18.35 cm^{-1}. For compound **2**, of the 14 066 reflections that were collected, 6726 were unique (R_{int} = 0.028) and 4761 with $I > 3\sigma(I)$ were used to solve the structure with SIR92. The final R values gave $R1$ = 0.044 for $I > 3\sigma(I)$, R = 0.061 and R_w = 0.116 for all data, with a linear absorption coefficient μ(Mo Kα) = 19.48 cm^{-1}. The non-hydrogen atoms were refined anisotropically. Hydrogen atoms were included but not refined. The pertinent crystallographic parameters are summarized in Table 1.

Thermogravimetric Measurements. Thermogravimetric data for **1** and **2** were collected on a Perkin-Elmer DSC-6 instrument over the 300−400 K temperature range under an N_2 gas atmosphere. The heating rate was fixed at 2 K min^{-1}.

Results and Discussion

Compounds **1** and **2** exist in the LS state at room temperature when they are synthesized in MeOH and $MeOH/CH_2Cl_2$ solutions, respectively. X-ray analysis was successfully carried out for compounds **1** and **2** at 200 and 230 K, respectively. Their selected bond distances and bond angles are listed in Table 2. Figures 1a and 2a show that when complexes **1** and **2** are in the LS state they crystallize in a triclinic $P\bar{1}$ space group. The single-crystal X-ray analyses of **1** and **2** revealed that each of the iron(III) atoms are octahedrally coordinated by four nitrogen atoms and two oxygen atoms in two qsal ligands, i.e., an N_4O_2 donor set. The values of the bond lengths are consistent with those for typical LS iron(III) compounds. The Fe−O distances are shorter than the Fe−N distances, which induce a pronounced distortion of the FeN_4O_2 octahedron. The qsal ligands form slightly distorted planes. The dihedral angles between the phenyl ring and the Fe−O(1)−N(1) chelate ring, between the other phenyl ring and the Fe−O(2)−N(3) chelate ring, between the quinoline ring and the Fe−N(1)−N(2) chelate ring, and between the other quinoline ring and the Fe−N(3)−N(4) chelate ring for **1** are 3.549°, 7.828°, 0.639°, and 2.928°, respectively. On the other hand, the dihedral angles between the phenyl ring and the Fe−O(1)−N(1) chelate ring, between the other phenyl ring and the Fe−O(2)−N(3) chelate ring, between the quinoline ring and the Fe−N(1)−N(2) chelate ring, and between the other quinoline ring and the Fe−N(3)−N(4) chelate ring for **2** are 2.430°, 9.518°, 0.684°, and 3.663°, respectively. The two tridentate ligands in the complexes are found to be nearly perpendicular to one another. The least-squares plane of the slightly distorted qsal ligands makes an angle of 79.49° and 80.44°, respectively, with one of the other qsal ligands for **1**

Table 1. Crystal Parameters for Compounds **1** and **2**

	1	**2**
formula	$C_{34}H_{26}O_3N_5Se_1Fe_1$	$C_{34}H_{24}O_2N_5Cl_2Se_1Fe_1$
formula weight	687.42	740.31
crystal system	triclinic	triclinic
space group	$P\bar{1}$ (No. 2)	$P\bar{1}$ (No. 2)
a/Å	11.179(3)	11.3501(2)
b/Å	13.744(2)	13.9252(5)
c/Å	9.894(2)	10.127(1)
α/deg	98.375(7)	98.327(6)
β/deg	106.540(7)	107.055(4)
γ/deg	84.202(7)	91.896(2)
V/Å^3	1438.9(5)	1509.3(2)
Z	2	2
D_{calc}/g cm^{-3}	1.587	1.629
$R1$	0.059	0.047
R	0.094	0.65
R_w	0.136	0.121

Table 2. Selected Bond Lengths (Å) and Angles (deg) for **1** and **2**

	1	**2**
	Bond Lengths	
Fe(1)−O(1)	1.871(6)	1.879(2)
Fe(1)−O(2)	1.869(6)	1.875(3)
Fe(1)−N(1)	1.949(7)	1.944(3)
Fe(1)−N(2)	1.976(7)	1.985(3)
Fe(1)−N(3)	1.941(7)	1.953(3)
Fe(1)−N(4)	1.971(7)	1.991(3)
	Bond Angles	
O(1)−Fe(1)−O(2)	93.8(3)	94.2(1)
O(1)−Fe(1)−N(1)	94.7(3)	94.6(1)
O(1)−Fe(1)−N(2)	175.7(3)	176.4(1)
O(1)−Fe(1)−N(3)	85.3(3)	85.4(1)
O(1)−Fe(1)−N(4)	90.4(3)	90.7(1)
O(2)−Fe(1)−N(1)	86.6(3)	87.7(1)
O(2)−Fe(1)−N(2)	89.9(3)	88.8(1)
O(2)−Fe(1)−N(3)	94.5(3)	94.0(1)
O(2)−Fe(1)−N(4)	175.1(3)	174.2(1)
N(1)−Fe(1)−N(2)	83.3(3)	83.6(1)
N(1)−Fe(1)−N(3)	179.0(3)	178.3(1)
N(1)−Fe(1)−N(4)	95.6(3)	95.1(1)
N(2)−Fe(1)−N(3)	96.6(3)	96.4(1)
N(2)−Fe(1)−N(4)	86.0(3)	86.4(1)
N(3)−Fe(1)−N(4)	83.3(3)	83.2(1)

(10) Dickinson, R. C.; Baker, W. A., Jr.; Collins, R. L. *J. Inorg. Nucl. Chem.* **1977**, *39*, 1531−1533.

(11) Oshio, H.; Kitazaki, K.; Mishiro, J.; Kato, N.; Maeda, Y.; Takashima, Y. *J. Chem. Soc., Dalton Trans.* **1987**, 1341−1347.

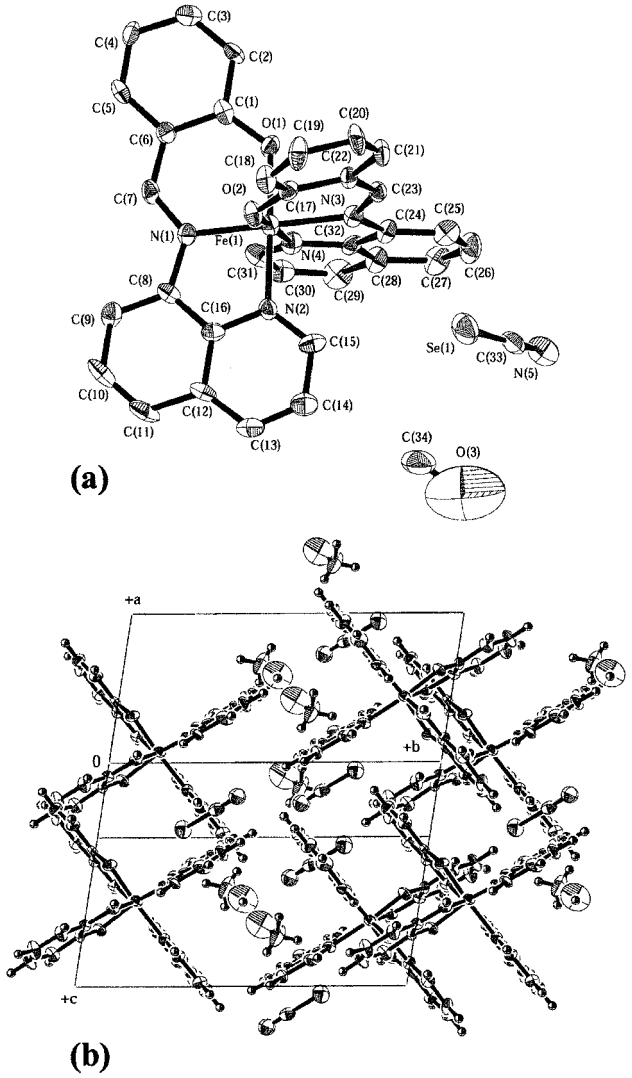

Figure 1. Molecular structures in the LS state at 200 K. (a) ORTEP view of **1** showing 50% probability displacement ellipsoids. (b) Structure of the $\pi-\pi$ stacking between complexes. Hydrogen atoms are omitted for clarity.

and **2**. The counteranion $NCSe^-$ and the solvent molecules are not located in the first coordination sphere. The crystal structures of the solvated **1** and **2** could not be determined in the HS form because the spin transition induces cracks in the crystal, making an X-ray single-crystal study impossible.

The temperature dependence of the magnetic susceptibility for the single crystals of **1** and **2** was measured at a rate of 2 K min^{-1} in the form of the χ_mT versus T curve, where χ_m is the molar magnetic susceptibility and T the temperature (Figures 3 and 4). The χ_mT value for **1** is 0.36 cm^3 K mol^{-1} at 150 K, which is in the range of values expected for the LS iron(III) ion. As the temperature is increased over 150 K, the χ_mT product remained practically constant from 150 to 320 K and then abruptly increased around $T_{1/2}\uparrow = 352$ K. The χ_mT value at 400 K was ca. 4.0 cm^3 K mol^{-1}, showing that the spin transition from the LS to the HS state was induced. The spin transition is directly related to the removal of solvent molecules. Thermogravimetry (Figure 5) carried out with the same heating rate (2 K min^{-1}) as for the magnetic susceptibility measurements revealed a continuous loss of mass, starting at room temperature. The decrease in mass proceeds rapidly in the temperature range 320−360 K. At 400 K, the mass lost is in exact agreement with the removal of a MeOH molecule. Elemental analysis also

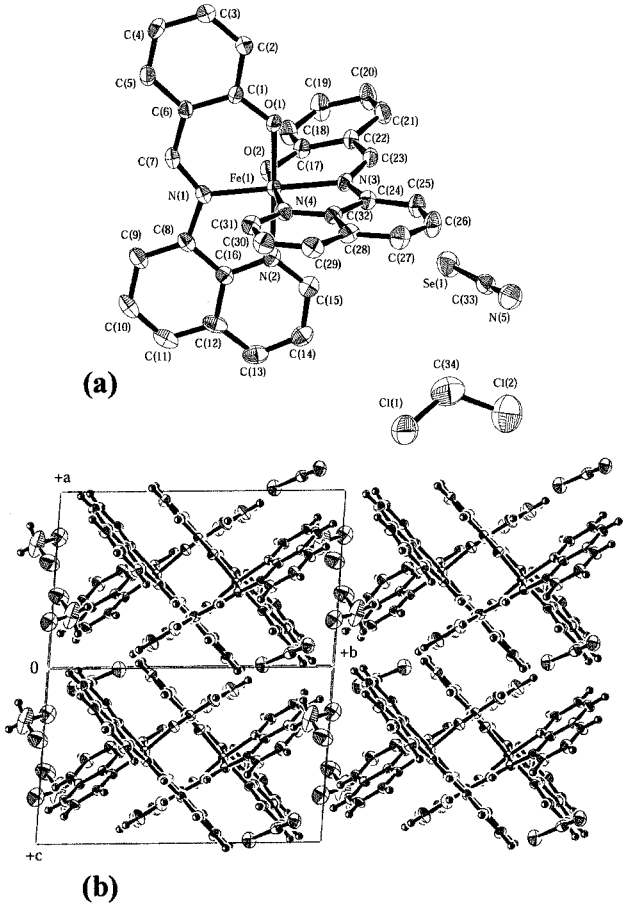

Figure 2. Molecular structures in the LS state at 230 K. (a) ORTEP view of **2** showing 50% probability displacement ellipsoids. (b) Structure of the $\pi-\pi$ stacking between complexes. Hydrogen atoms are omitted for clarity.

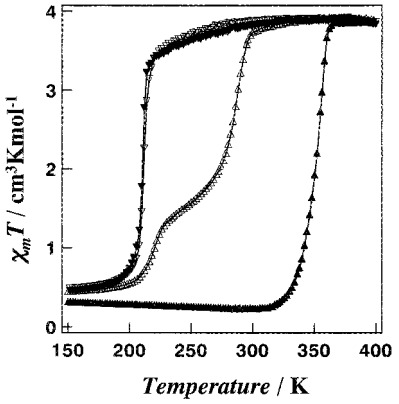

Figure 3. χ_mT versus T plots for **1**. The sample was warmed from 5 to 400 K (▲) and then cooled from 400 to 5 K (▼) in the first cycle, and then the sample was warmed from 5 to 400 K (△) and then cooled from 400 to 5 K (▽) in the second cycle at a rate of 2 K min^{-1}.

supports the idea that the first hysteresis loop of 140 K ($T_{1/2}\uparrow =$ 352 K and $T_{1/2}\downarrow = 212$ K) is an apparent one. Note that a similar large apparent hysteresis has been reported for $[Fe(hyetrz)_3](3\text{-nitrophenylsulfonate})_2\cdot 3H_2O$ by Garcia et al.[12,13] On cooling, the χ_mT value for the nonsolvated compound **1** was almost constant from 400 to 220 K and then abruptly dropped around $T_{1/2}\downarrow = 212$ K, showing that the HS moieties were restored to the LS state. A second heating experiment revealed that the spin-crossover takes place in a two-step manner.[14−17] The so-called "step 1" and "step 2" are centered around the temperatures

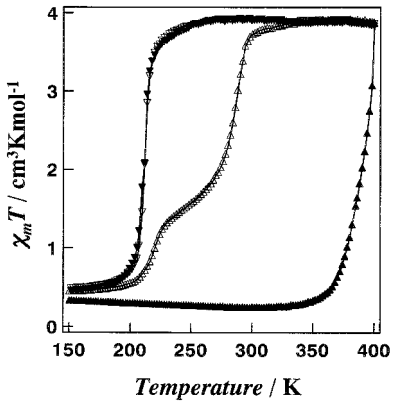

Figure 4. $\chi_m T$ versus T plots for **2**. The sample was warmed from 5 to 400 K (▲) and then cooled from 400 to 5 K (▼) in the first cycle, and then the sample was warmed from 5 to 400 K (△) and then cooled from 400 to 5 K (▽) in the second cycle at a rate of 2 K min^{-1}.

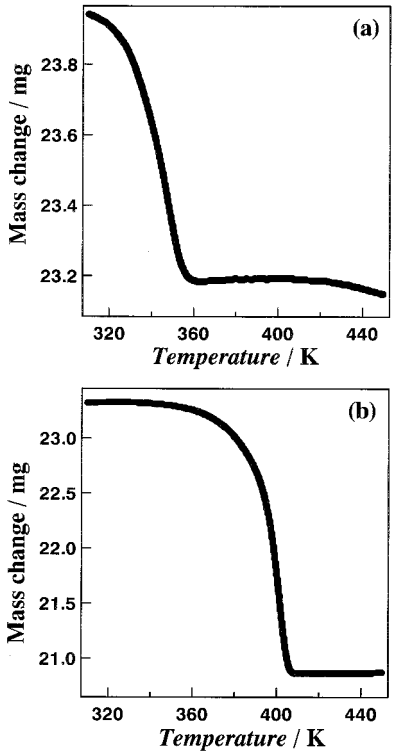

Figure 5. Thermogravimetric analysis (a) for **1** and (b) for **2**.

$T_{1/2(S1)}\uparrow$ = 215 K and $T_{1/2(S2)}\uparrow$ = 282 K, respectively. The magnetic behavior shows that the upper step, step 2, is about twice as high as the lower step, step 1. Additional thermal cycles did not modify the thermal hysteresis loop. The $\chi_m T$ value at the inflection point around 250 K is 1.6 cm^3 K mol^{-1}. When the hysteresis widths (ΔT) in steps 1 and 2 are defined as the difference between $T_{1/2(S1)}\uparrow$ and $T_{1/2}\downarrow$, and $T_{1/2(S2)}\uparrow$ and $T_{1/2}\downarrow$, respectively, they can be estimated to be 3 K (step 1) and 70 K (step 2). Compound **2** also exhibits spin-crossover behavior with an apparent hysteresis loop of 180 K ($T_{1/2}\uparrow$ = 392 K and $T_{1/2}\downarrow$ = 212 K). The decrease in mass proceeds rapidly in the temperature range 380−400 K (Figure 5b). At 420 K the mass lost is in exact agreement with the removal of a CH_2Cl_2 molecule. Elemental analysis also supports this idea. Additional heating and cooling cycles show that the nonsolvated compound **2** exhibits the same asymmetrical hysteresis as that for the nonsolvated compound **1** ($T_{1/2(S1)}\uparrow$ = 215 K, $T_{1/2(S2)}\uparrow$ = 282 K, and $T_{1/2}\downarrow$ = 212 K).

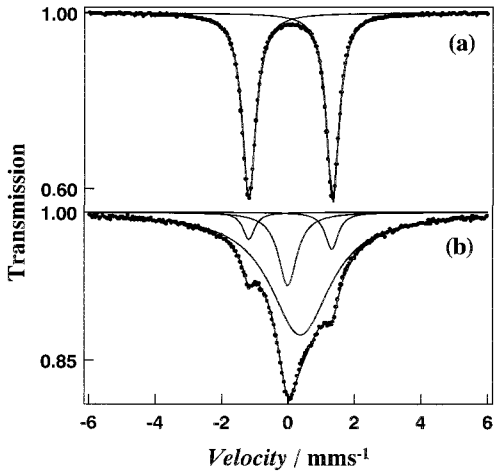

Figure 6. ^{57}Fe Mössbauer spectra at room temperature (a) before and (b) after annealing at 400 K for **1**. There is a small amount of LS form in the HS form after annealing, indicating that solvent molecules are still retained.

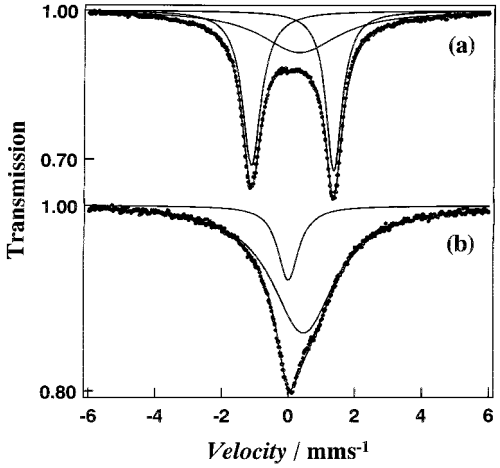

Figure 7. ^{57}Fe Mössbauer spectra at room temperature (a) before and (b) after annealing at 400 K for **2**. There is a small amount of HS form in the LS form before annealing, indicating the removal of a small amount of solvent molecules.

To confirm the induction of the spin-crossover, Mössbauer spectra for **1** and **2** were measured at room temperature before and after annealing at 400 K (Figures 6 and 7). The complexes were synthesized by using ^{57}Fe to enhance the Mössbauer signal. Before annealing for **1**, a wide doublet with QS (quadrupole splitting) = 2.52 mm s^{-1} and IS (isomer shift) = 0.07 mm s^{-1} was observed at room temperature, which corresponded to the LS state of iron(III) compounds. After annealing at 400 K for **1**, a broad singlet with QS = 0.38 mm s^{-1} and IS = 0.25 mm s^{-1} was observed at room temperature, showing that the iron(III) takes the HS state. Mössbauer spectra similar to those for **1** before and after annealing at 400 K were observed for **2** at room temperature, i.e., QS = 2.47 mm s^{-1} and IS = 0.11 mm s^{-1} before annealing, and QS = 0.46 mm s^{-1} and IS = 0.23 mm s^{-1} after annealing. This is consistent with the magnetic properties described above.

It should be noted that several examples of the two-step spin transition have been reported.[14−24] Compared with these ex-

(12) Garcia, Y.; Koningsbruggen, P. J. V.; Codjovi, E.; Lapouyade, R.; Kahn, O.; Rabardel, L. *J. Mater. Chem.* **1997**, *7*, 857−858.
(13) Garcia, Y.; Koningsbruggen, P. J.; Lapouyade, R.; Fournès, L.; Rabardel, L.; Kahn, O.; Ksenofontov, V.; Levchenko, G.; Gütlich, P. *Chem. Mater.* **1998**, *10*, 2426−2433.

amples, the present compounds have the following important characteristics: (I) the spin transition shows a hysteresis loop and (II) the two-step spin-crossover is observed only in the warming mode. To the best our knowledge, this kind of hysteresis behavior has not been reported previously. Furthermore, the hysteresis width of 70 K in step 2 is quite wide, compared with those reported elsewhere. The abrupt phase transition with the hysteresis effect suggests that a strong intermolecular interaction operates in this complex.[8] Through careful investigation of the intermolecular arrangement in the analyzed crystal structure, it was found that $[Fe(qsal)_2]^+$ cations form $\pi-\pi$ stacking in the qsal ligands between the quinoline and phenyl rings, forming a one-dimensional network for **1** and **2** (Figures 1b and 2b). As described above, the dihedral angles of the two ligands on the iron(III) ion are different from each other. When the ligands with smaller and larger dihedral angles are represented as ligands A and B, it was found that ligand A always interacts with ligand A on the neighboring complexes in the *ac* plane and ligand B always interacts with the neighboring ligand B, respectively. That is, when either complex **1** or **2** is represented by (A:Fe:B), the molecular arrangement can be expressed simply by ···(B:Fe:A)(A:Fe:B)(B:Fe:A)-(A:Fe:B)(B:Fe:A)(A:Fe:B)···. For **1**, the distances between the quinoline and the phenyl rings of its nearest neighbor A and B, i.e., A_q- - -A_p and B_q- - -B_p, are 3.35 and 3.43 Å, respectively. On the other hand, the distances of A_q- - -A_p and B_q- - -B_p for **2** are 3.35 and 3.52 Å, respectively. Furthermore, it was found that there is a molecular stacking between the phenyl rings in the qsal ligands, by which the one-dimensional molecular assemblies form a two-dimensional sheet structure. The distances between the phenyl rings, A_p- - -A_p and B_p- - -B_p, for **1** are 3.51 and 3.69 Å, respectively. On the other hand, the distances, A_p- - -A_p and B_p- - -B_p, for **2** are 3.46 and 3.98 Å, respectively. The distances between the two-dimensional sheets for **1** and **2** are 13.75 and 14.04 Å, respectively. The $NCSe^-$ and the solvent molecules are located between the two-dimensional sheets. Note that the overlap between the quinoline and the phenyl rings is much greater than that between the phenyl rings. This means that the one-dimensional character is rather strong in the molecular arrangements, although the $[Fe(qsal)_2]^+$ cations appear to form a two-dimensional sheet structure. The molecular arrangements described here suggest that the cooperativity operating in nonsolvated compounds **1** and **2** arises mainly from the intermolecular $\pi-\pi$ interactions between the quinoline and phenyl rings. Other intermolecular interactions such as direct contacts between $[Fe(qsal)_2]^+$ cations and $NCSe^-$ counteranions (2.57 Å) may also play an important role in the strong cooperativity.

It is useful to compare the hysteresis width of the nonsolvated complexes **1** and **2** with those reported previously.[12−31] Several compounds with a polymeric structure have been found to display a wide thermal hysteresis.[25−27] Kahn et al. reported that an iron(II) compound, $[Fe(Htrz)_{3-3x}(4\text{-}NH_2trz)_{3x}](ClO_4)_2 \cdot nH_2O$ ($x = 0.05$) (Htrz = 1,2,4-1*H*-triazole, 4-NH_2trz = 4-amino-1,2,4-triazole), which has a polymeric structure, displays a thermal hysteresis at room temperature ($T_{1/2}\uparrow = 304$ K and $T_{1/2}\downarrow = 288$ K).[18,19] However, the polymeric compound is not strictly molecular, as was concluded by previous studies.[12,13,25−27] Several mononuclear molecules have also exhibited wide thermal hysteresis loops.[28−31] The maximum hysteresis width observed for iron(II) complexes with intermolecular $\pi-\pi$ interactions is 40 K,[28−30] which is narrower that observed for the nonsolvated complexes **1** and **2**. Furthermore, it has been reported that the iron(II) compound, $[Fe(2\text{-}pic)_3]Cl_2 \cdot H_2O$ (2-pic = 2-picolylamine),[32,33] exhibits the widest thermal hysteresis loop of 91 K with $T_{1/2}\uparrow = 295$ K and $T_{1/2}\downarrow$ _= 204 K, respectively. Note that the structure of the compound has not been fully analyzed as yet. These previous results show that the hysteresis width of 70 K presented here is one of the widest values among the spin-crossover complexes reported so far.[12−31]

Finally, we would like to comment on the asymmetrical hysteresis observed in the nonsolvated complexes **1** and **2**. The molecular arrangement that exists in the *ac* plane, ···(B:Fe:A)-(A:Fe:B)(B:Fe:A)(A:Fe:B)(B:Fe:A)(A:Fe:B)···, shows that there are two kinds of interactions between complex **1** or between complex **2**, i.e., the $\pi-\pi$ interactions between the A ligands and the ones between the B ligands. The distance between the quinoline and the phenyl rings, A_q- - -A_p, is shorter than the distance B_q- - -B_p, indicating that the molecular interactions via A_q- - -A_p in the one-dimensional network are stronger than those via B_q- - -B_p. This means that the complexes can be treated as a dimer, such as ···[(B:Fe:A)(A:Fe:B)][(B:Fe:A)(A:Fe:B)]-[(B:Fe:A)(A:Fe:B)]···, where the dimer is represented by [(B:Fe:A)(A:Fe:B)]. Assuming that the dimer structure is retained after the loss of the solvents, the spin-transition behavior might be simulated by the dinuclear model reported by Kahn and Real et al.[15,34] Note that these authors have succeeded in explaining a two-step transition in an iron(II) dinuclear species in a theoretical manner. Because they have given detailed discussions on the model, it is described here only briefly. The spin transition process in [(B:Fe:A)(A:Fe:B)] can be schematized as [(LS),(LS)](x) ↔ [(HS),(LS)](y) ↔ [(HS),(HS)](z), where x, y, and z are the molar fractions of each of the spin isomers, with $x + y + z = 1$. The enthalpy and entropy of [(LS),(LS)],

(14) Köppen, H.; Müller, E. W.; Köhler, C. P.; Spiering, H.; Meissner, E.; Gütlich, P. *Chem. Phys. Lett.* **1982**, *91*, 348.
(15) Real, J. A.; Bolvin, H.; Bousseksou, A.; Dworkin, A.; Kahn, O.; Varret, F.; Zarembowitch, J. *J. Am. Chem. Soc.* **1992**, *114*, 4650−4658.
(16) Jacobi, R.; Spiering, H.; Gütlich, P. *J. Phys. Chem. Solids* **1992**, *53*, 267−275.
(17) Bousseksou, A.; Nasser, J.; Linares, J.; Boukheddaden, K.; Varret, F. *J. Phys. I (France)* **1992**, *2*, 1381−1403.
(18) Bousseksou, A.; Varret, F.; Nasser, J. *J. Phys. I (France)* **1993**, *3*, 1463−1473.
(19) Boinnard, D.; Bousseksou, A.; Dworkin, A.; Savariault, J.-M.; Varret, F.; Tuchagues, J.-P. *Inorg. Chem.* **1994**, *33*, 271−281.
(20) Bousseksou, A.; Nasser, J.; Varret, F. *J. Magn. Magn. Mater.* **1995**, *140−144*, 1511−1512.
(21) Buchen, T.; Schollmeyer, D.; Gütlich, P. *Inorg. Chem.* **1996**, *35*, 155−161.
(22) Real, J. A.; Castro, I.; Bousseksou, A.; Verdaguer, M.; Burriel, R.; Linares, J.; Varret, F. *Inorg. Chem.* **1997**, *36*, 455−464.
(23) Spiering, H.; Kohlhaas, T.; Romstedt, H.; Hauser, A.; Bruns-Yilmaz, C.; Kusz, J.; Gütlich, P. *Coord. Chem. Rev.* **1999**, *190−192*, 629−647.
(24) Simaan, A. J.; Boillot, M.-L.; Rivière, E.; Boussac, A.; Girerd, J.-J. *Angew. Chem., Int. Ed.* **2000**, *39*, 196−198.
(25) Kröber, J.; Codjovi, E.; Kahn, O.; Grolière, F.; Jay, C. *J. Am. Chem. Soc.* **1993**, *115*, 9810−9811.
(26) Kröber, J.; Audière, J.-P.; Claude, R.; Codjovi, E.; Kahn, O.; Haasnoot, J. G.; Grolière, F.; Jay, C. *Chem. Mater.* **1994**, *6*, 1404−1412.
(27) Koningsbruggen, P. J. V.; Garcia, Y.; Codjovi, E.; Lapouyade, R.; Kahn, O.; Fournès, L.; Rabardel, L. *J. Mater. Chem.* **1997**, *7*, 2069−2075.
(28) Létard, J.-F.; Guionneau, P.; Codjovi, E.; Lavastre, O.; Bravic, G.; Chasseau, D.; Kahn, O. *J. Am. Chem. Soc.* **1997**, *119*, 10861−10862.
(29) Létard, J.-F.; Guionneau, P.; Rabardel, L.; Howard, J. A. K.; Goeta, A. E.; Chasseau, D.; Kahn, O. *Inorg. Chem.* **1998**, *37*, 4432−4441.
(30) Zhong, Z. J.; Tao, J. Q.; Yu, Z.; Dun, C. Y.; Liu, Y. J.; You, X. Z. *J. Chem. Soc., Dalton Trans.* **1998**, 327−328.
(31) Létard, J.-F.; Real, J. A.; Moliner, N.; Gaspar, A. B.; Capes, L.; Cador, O.; Kahn, O. *J. Am. Chem. Soc.* **1999**, *121*, 10630−10631.
(32) Sorai, M.; Ensling, J.; Gütlich, P. *Chem. Phys.* **1976**, *18*, 199−209.
(33) Sorai, M.; Ensling, J.; Hasselbach, K. M.; Gütlich, P. *Chem. Phys.* **1977**, *20*, 197−208.
(34) (a) Kahn, O.; Launay, J. P. *Chemtronics* **1988**, *3*, 140. (b) Zarembowitch, J.; Kahn, O. *New J. Chem.* **1991**, *15*, 181. Kahn, O. *Molecular Magnetism*; VCH: New York, 1993.

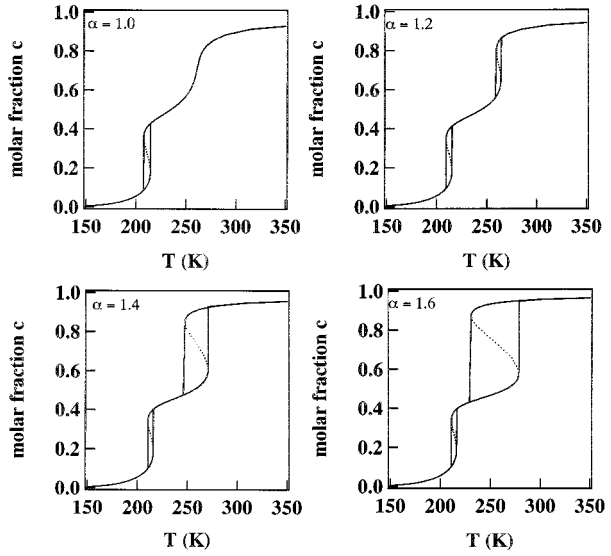

Figure 8. High-spin molar fraction c versus T curves for $\Delta H = 1175$ cm^{-1}, $\Delta S = 5$ cm^{-1}, $W = -50$ cm^{-1}, $\gamma = 332$ cm^{-1}, $\beta = 2$, and $\alpha = 1$, 1.2, 1.4, and 1.6.

[(HS),(LS)], and [(HS),(HS)] are noted as $H_{LS,LS}$, $H_{HS,LS}$, $H_{HS,HS}$ and $S_{LS,LS}$, $S_{HS,LS}$, $S_{HS,HS}$, respectively. The $H_{HS,LS}$ value is equal to $(\Delta H/2) + W$, where $\Delta H = (H_{HS,HS} - H_{LS,LS})$ and W (a small positive or negative correction with regard to $\Delta H/2$) is the interaction parameter in the dimer. Furthermore, it is assumed that both entropy variations $S_{HS,HS} - S_{HS,LS}$ and $S_{HS,LS} - S_{LS,LS}$ are equal to $\Delta S = (S_{HS,HS} - S_{LS,LS})/2$. The Gibbs free energy of the system is given by $G = xG_{LS,LS} + yG_{HS,LS} + zG_{LS,LS} + \Gamma + RT(x \ln x + y \ln y + z \ln z)$, where $G_{LS,LS}$, $G_{HS,LS}$, and $G_{HS,HS}$ are the molar Gibbs free energies of [(LS),(LS)], [(HS),(LS)], and [(HS),(HS)], respectively, and Γ accounts for the excess Gibbs energy due to the molecular interactions. The general expression is that Γ is equal to $\gamma(xy + \alpha yz + \beta zx)$, where γ, $\gamma\alpha$, and $\gamma\beta$ denote the interaction parameters between [(LS),(LS)] and [(HS),(LS)], between [(HS),(LS)] and [(HS),(HS)], and between [(LS),(LS)] and [(HS),(HS)], respectively. The equilibrium conditions are given by

$$\left(\frac{\partial G(x,y)}{\partial x}\right)_T = 0 \qquad \text{and} \qquad \left(\frac{\partial G(x,y)}{\partial y}\right)_T = 0 \qquad (1)$$

The molar fraction of iron(III) ions in the HS state, c, is equal to $(y + 2z)/2$, which can be calculated from (1) by looking for the minima of G at various temperatures.

To explain a conventional two-step transition, Real et al. choose the parameter $\alpha = 1$.[15] That is, the interaction parameters between [(HS),(HS)] and [(HS),(LS)] and between [(HS),(LS)] and [(LS),(LS)] are equivalent to each other. On the other hand, the appearance of the asymmetrical hysteresis suggests that the interaction parameters in compounds **1** and **2** should be different from each other. Hence, we have quantitatively investigated the spin-transition behavior for different values of α, namely 1, 1.2, 1.4, and 1.6. Figure 8 shows the c vs T curves under the conditions in (1). ΔH, ΔS, W, γ, and β are assumed to be 1175 cm^{-1}, 5 cm^{-1}, -50 cm^{-1}, 332 cm^{-1}, and 2, respectively. The choice of the negative value for W implies that an asymmetric energy level scheme for three [(LS),(LS)], [(HS),(LS)], and [(HS),(HS)] states is introduced such that [(HS),(LS)] state is stabilized in energy.[15,23] This means that an antiferromagnetic type of short-range interaction, i.e., an interaction favoring inhomogeneous [(HS),(LS)] states, operates in the dimer. Hence, it is expected that a ferromagnetic type of interaction, i.e., an interaction favoring homogeneous phases with dominating LS or HS character, and the antiferromagnetic type of interaction compete with each other in the compounds, leading to the induction of synergistic effects. Note that Kahn and Real et al. show a two-step transition by using the parameters $\Delta H = 1000$ cm^{-1}, $\Delta S = 5$ cm^{-1}, $W = -50$ cm^{-1}, $\gamma = 332$ cm^{-1}, and $\beta = 2$.[15] Figure 8 shows the c vs T curves under the conditions in (1). As shown in Figure 8, a two-step transition is observed in any case. In the case of $\alpha = 1$, hysteresis is observed only for the low-temperature step, while it is observed in both the low-temperature and high-temperature steps for $\alpha = 1.2$, 1.4, and 1.6. It is found that the hysteresis width in the high-temperature step increases with increasing α. This behavior suggests that an appropriate choice of the parameters including α might allow one to follow the asymmetrical hysteresis loop. In fact, an agreement between the calculated and the experimental curves is obtained for $\Delta H = 1175$ cm^{-1}, $\Delta S = 5$ cm^{-1}, $W = -50$ cm^{-1}, $\gamma = 332$ cm^{-1}, $\alpha = 1.7$, and $\beta = 2.4$. As shown in Figure 9, the spin-transition temperatures in the cooling and warming modes in the high-temperature step are lower and higher, respectively, than those in the low-temperature steps, which results in the hysteresis shape with one step in the cooling mode and two steps in the warming mode.

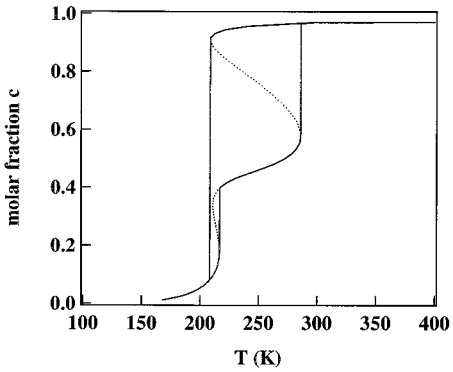

Figure 9. Calculated temperature dependence of the high-spin molar fraction c (see text).

The quantitative investigations presented above show that asymmetrical hysteresis appears when the value of the interaction parameter, α, is not equal to 1. This condition is not a special one, because, in general, the interactions between [(HS),(HS)] and [(HS),(LS)] and between [(HS),(LS)] and [(LS),(LS)] should be different from each other to some degree. It is natural that this is the case for compounds **1** and **2**. This suggests that, although the shape of the hysteresis loop reported in this work is novel and it is an unusual phenomenon, it is still a theoretically possible one.

It should be noted that the two-step transition could be observed in the following cases as well. (1) The compounds have a low-symmetry structure with nonequivalent crystallographic sites. (2) The complexes sit on equivalent lattice sites, but strong nearest-neighbor interactions operate in the compounds, leading to the formation superstructures and correlations. (3) The compounds exhibit the spin transition coupled to a crystallographic phase transition. Hence, the above interpretation for the asymmetrical hysteresis with a two-step warming mode and a one-step cooling mode might be not a unique one, but a possible explanation. To investigate further the exact microscopic origin of the asymmetrical hysteresis, additional characterization, especially the measurement of the variable-temperature single-crystal structures of the nonsolvated **1** or **2**, is required. Furthermore, the symmetry relationships and

eventual symmetry breaking between the spin-crossover sites should be investigated.

In summary, we have shown that $[Fe(qsal)_2]NCSe\cdot MeOH$ (**1**) and $[Fe(qsal)_2]NCSe\cdot CH_2Cl_2$ (**2**) display a wide apparent hysteresis in the first cycle. After the first cycle, they show a two-step transition in the warming mode and a one-step transition in the cooling mode. The hysteresis width in step 2 after the first cycle is 70 K, which is one of the largest hysteresis effects reported so far. Using the model reported by Kahn and Real et al.,[15,34] we could simulate the asymmetrical hysteresis loop.

Acknowledgment. This work was supported in part by a Joint Research Project for Regional Intensive of Kanagawa Prefecture. We thank Prof. D. Tryk for reading the manuscript.

Supporting Information Available: Tables giving crystallographic data, positional parameters, and *U* values (CIF). This material is available free of charge via the Internet at http://pubs.acs.org.

JA0017920